**Title**
Setting up C-13 CP/MAS experiments



**Journal**
Concepts in Magnetic Resonance Part A, 22A(1)

**ISSN**
1546-6086

**Author**
Taylor, Robert E

**Publication Date**
2004-05-01

Peer reviewed

# Setting Up $^{13}$C CP/MAS Experiments

R. E. Taylor
Department of Chemistry and Biochemistry
University of California, Los Angeles
Los Angeles, CA 90095

Correspondence to: Dr. R. Taylor; Email: taylor@chem.ucla.edu

ABSTRACT:

The $^{13}$C cross-polarization (CP) technique combined with magic angle spinning (MAS) has become one of the more commonly performed solid-state nuclear magnetic resonance (NMR) experiments. The basics of initially setting up the experiment are given and used to illustrate such NMR phenomena as rotational echoes, homogeneous and inhomogeneous interactions, continuous wave $^{1}$H decoupling, and coupling of quadrupolar $^{14}$N nuclei to $^{13}$C nuclei. The polarization transfer from the protons to the carbons is briefly described with the usual thermodynamic and quantum mechanical models. The setup and use of the experiment for routine analyses are discussed.

KEY WORDS:

solid-state NMR; $^{13}$C CP/MAS; cross-polarization; magic angle spinning; solid-state chemical shift calibration; $^{79}$Br MAS.

## INTRODUCTION

The combination (1) of the $^{13}$C cross-polarization (CP) technique (2) with magic angle spinning (MAS) (3,4) has become one of the more commonly performed solid-state nuclear magnetic resonance (NMR) experiments. This one dimensional experiment offers high-sensitivity spectra of natural abundance $^{13}$C in solids by polarization transfer from abundant proton spins and by eliminating broadening from chemical shift anisotropy and dipolar coupling. The theory and experiment have been described numerous times (5-10). A notably useful discussion of the practical aspects of the experiment, such as contact times and quantification, has been given by Voelkel (11). Current developments and applications of the technique can be found in such annual reviews of the literature as "A Specialist Periodical Report - Nuclear Magnetic Resonance" (12).

The application of solid-state NMR techniques usually arises due to specific interest in the physics of the solid state, including packing effects, polymorphic structures, molecular dynamics, or an interest in solid-state reactions. Sometimes, the application is motivated by an inability to dissolve the material of interest. The cross-polarization

technique for $^{13}C$ is usually chosen over a simple single-pulse experiment for the sensitivity enhancement, which is due to both the polarization transfer from the protons to the carbons and to the short(er) relaxation times of protons. The high resolution of a rare-spin species is retained by the direct observation of the $^{13}C$ spins, as opposed to the indirect detection techniques used routinely in solution-state NMR. Errors in setting up the $^{13}C$ CP/MAS experiment normally result in losses of sensitivity and resolution. The purpose of this paper is to provide assistance in setting up the experiment on a suitable spectrometer for the first time (and thus avoiding errors). These techniques are commonly used in many labs to set up the experiment and to check spectrometer performance.

## EXPERIMENTAL SETUP

Generally the setup of any NMR experiment begins with the observation of a spectrum from a suitable standard(s). Factors that dictate the choice of standards include availability, ease of handling, and a spectrum that is easily observable in a single scan to allow the easy adjustment of parameters.

### $^{79}$Br MAS

The initial setup of a $^{13}C$ CP/MAS experiment typically begins with the observation of a $^{79}Br$ MAS spectrum (13) of potassium bromide, KBr. One might reasonably ask why a $^{79}Br$ experiment is first run when the setup of a $^{13}C$ experiment is desired. The reasons are twofold. First, the angle of the sample's rotation axis can be accurately adjusted to the magic angle relative to magnetic field. Indeed the deviation from the magic angle can be quantified by comparison of average height of the second-order spinning sidebands with the height of the central peak in the bromine spectrum (13). Second, the $^{79}Br$ resonance can be used as a "lock" to set the magnetic field to the same value in future experiments.

There are several reasons for the specific choice of $^{79}Br$ MAS on KBr. Since the $^{79}Br$ nuclei are abundant half-integer (I=3/2) spins with a moderate quadrupole moment and have a magnetogyric ratio very close to that of $^{13}C$, the only hardware change usually required to observe both nuclei is a small adjustment in the tuning of the probe. With KBr having a face-centered cubic structure (14), the quadrupolar coupling is zero and will yield a relatively narrow line in the spectrum. (Bromine sites with a non-zero quadrupolar coupling arise from sites near crystallographic defects.) The abundance along with the cubic symmetry leads to high sensitivity. The high sensitivity, in combination with the convenience of a magnetogyric ratio very close to that of $^{13}C$, motivates the choice of $^{79}Br$ MAS on KBr.

The experimental parameters for $^{79}Br$ observation are first set. For example, the observation frequency for the nucleus may be set by determining the frequency from an appropriate table or reference book (15). On many commercial spectrometers such

information may be provided directly by the spectrometer software. The probe should be tuned to this frequency.

The pulse program for data acquisition is simply a single pulse followed by data acquisition of the time domain signal. Such an acquisition of a free induction decay (FID) is shown schematically in Figure 1. The FID is so named because it is a free (of radiofrequency pulses) precession signal that decays. For quadrature detection, the spectral width on many commercial spectrometers is defined as SW = 1/(2*DW), where DW is the dwell time. Thus, a spectral width of 125,000 or 100,000 Hz corresponds to a dwell time of 4 or 5 microseconds (μs).

Before data acquisition, the KBr must be packed in a rotor (shown in Figure 2) for sample spinning. Since the KBr and the other standards used to set up these experiments are polycrystalline powders (or can be ground into such with a mortar and pestle), the sample packing in rotors suitable for high speed rotation is fairly easy. Usually a uniform packing suffices. However, other samples which are not easily made uniform may prove to be more of a challenge to spin stably. Other preparation techniques may be required to make the samples spin stably. For example, a thin film polymer may simply be rolled up into a cylinder and cut to a size to fit into the rotor. A polymer sheet may be punched with an appropriate size cork borer, in a manner much the same as one uses a cookie cutter. The polymer disks may then be stacked in the rotor perpendicular to the axis of rotation. If the sample consists of larger chunks which cannot be easily ground with a mortar and pestle, the problem of voids (i.e., non-uniform density) can be ameliorated by adding an inert filler. As a specific example, consider a sample of polymer pellets that is not water soluble. If $^{13}C$ CP/MAS is the desired experiment, one might add ground sodium chloride to the rotor to fill the voids left by the pellets. This filler would add no background signal and can be easily removed afterwards simply by rinsing the sample with water.

For data acquisition with one scan, the number of data points to acquire is selected so that the total acquisition time is around 16 milliseconds (ms). The 16 ms are adequate to fully acquire the decay of the $^{79}Br$ signal into the noise. The recycle delay between scans can be set at 0.25 seconds. A short pulse width, typically 2 to 4 μs depending upon the probe, is used. The spectrum of KBr spun at approximately 5 kHz can usually be acquired easily in one scan on most spectrometers. A stator for magic angle spinning based on a double air bearing design is shown in Figure 3 with the doubly-tuned single coil probe shown in Figure 4. Of course a stable static magnetic field is needed. If the spectrometer has a lock sweep function for use with solution NMR, then this must be shut off, as no deuterated solvents are used as a field lock in solid-state NMR.

Once the $^{79}Br$ signal is found, the signal can be maximized by either increasing the duration of the pulse width or increasing the pulse power. Then the $^{79}Br$ observation frequency can be set on resonance. Of course only one signal can be set on resonance at a given time. In the case of angle set-up, the central transition of KBr is set on resonance. "On resonance" in the time domain simply means observing a single exponential decay (as opposed to a decaying cosine wave). The receiver phase may be adjusted so that the KBr peak is on resonance in the time domain as indicated by the decaying exponential signal (ignoring the "spikes" for the moment), as shown in Figure 5. In the frequency domain this is equivalent to the central transition of KBr being in the center of the full

spectrum (and not just in the center of an expansion of the spectrum). This is illustrated in Figure 6.

The angle between the axis of sample rotation and the static magnetic field can be adjusted to the magic angle by maximizing both the number of spikes observed in the $^{79}$Br spectrum and their amplitudes. If the angle is adjusted away from the magic angle, few or no spikes are observed. In the $^{79}$Br spectrum, this can lead to a marked broadening and a decrease in the intensity of the sideband manifold. As mentioned earlier, the deviation from the magic angle can be quantified by measuring the ratio R of the average height of the second-order spinning sidebands (since the first spinning sideband is less sensitive to the angle) with the height of the central peak (13). At the magic angle, one typically measures a minimum for R in the high teens to almost twenty. Even at 0.1 degree deviation, this ratio increases. For a 0.5 degree deviation, the ratio R typically increases to the range of 40 to 80. The variation in R results from whether powdered or large crystals of KBr are used. Simply by looking at this ratio the angle can usually be set to within 0.1 degree.

The "spikes" on the $^{79}$Br free induction decay are simply the rotational echoes (16), which Lowe (4) "facetiously call(ed) ... 'spinning echoes'." These rotational echoes are the result of the magnetization being refocused upon each rotor revolution. This can easily be demonstrated by noticing how these "spikes" behave as a function of the spinning speed of the rotor, as illustrated in Figure 7. As the spinning speed is reduced from 5 kHz (top trace) to the 2.5 kHz (bottom), these echoes separate further in time in the FID as it takes longer for each rotor revolution. These rotational echoes are the modulations in the time domain which give rise to the observed spinning sidebands in the frequency domain after Fourier transformation.

It is also interesting to note that in the frequency spectrum, while the spinning sidebands are separated from each other by the rotation frequency, the spinning sidebands are not symmetric with respect to the center band of the $^{79}$Br signal. This shift of the first two spinning sidebands relative to the center band is shown in Figure 8. With the central transition arbitrarily assigned a shift of zero ppm, the first two spinning sidebands are at 5014 Hz and -4991 Hz. This shift is greater than the digitial resolution of the spectrum of 1.5 Hz/point. While KBr has cubic symmetry (which makes the quadrupolar interaction zero), the spinning sidebands show a small frequency shift relative to the center band due to the second order quadrupolar interaction. This arises as strain and imperfections in real crystals cause deviations from perfect cubic symmetry.

In summary, the angle of sample rotation can be adjusted to the magic angle by maximizing the number and amplitude of the rotational echoes observed in the $^{79}$Br MAS signal from KBr. By saving this KBr dataset, the static magnetic field can be adjusted (as opposed to adjusting the stored radiofrequency used for observation) in order to bring the signal back to resonance to compensate for any drift of the magnet. As a result, the parameters or data files obtained below for $^{13}$C cross-polarization can be used as is without the need for updating frequencies due to magnet drift. That is, the $^{79}$Br MAS signal can be used to keep the magnet "locked" to the correct magnetic field value, much the same as one uses the deuterium signal from the solvent in high resolution solution NMR. Of course this is not an active lock under continuous control as usually found for deuterium on solution-state spectrometers. Never the less, it does provide the ability to check the magnetic field between experiments and to adjust as necessary.

## $^{1}$H MAS

The second step is to observe the $^{1}$H MAS spectrum of adamantane, $C_{10}H_{16}$. Again, the reasons are twofold. The first is to determine the resonance frequency of the protons. The second is to measure the $^{1}$H ninety degree pulse. The particular choice of adamantane as a standard is due to the fact that the proton signal is easily detected. Since even moderate spinning speeds at the magic angle begin to average the homonuclear proton dipolar interaction, the length of the proton FID is significantly increased over that of the static sample. This lengthening of the FID in time avoids problems associated with the acquisition of a rapid signal decay due to a broad line. Adamantane is also used since it will give a $^{13}$C CP/MAS signal which is usually easily seen on one scan.

The experimental parameters for $^{1}$H NMR observation must be set, e.g. the observation frequency for protons. Before data acquisition, the $^{1}$H channel of the probe must be tuned. The pulse program is the same single pulse followed by data acquisition used for $^{79}$Br MAS. The pulse width may be set to 4 μs or whatever is appropriate for the probe being used. The idea is to adjust the proton power using a short pulse (to minimize possible damage to the probe from high radiofrequency power) to an appropriate setting that can also be used for the $^{1}$H decoupling in later experiments. Using a spectral width of 100,000 or 125,000 Hz, an acquisition time of 4 ms should be sufficient to acquire the FID without signal truncation. A recycle delay of 3 seconds can be used. A $^{1}$H MAS spectrum from a rotor full of adamantane spinning at 5 kHz should be easily acquired in one scan on most spectrometers. The observation frequency can be adjusted so that it is on resonance. The $^{1}$H ninety degree pulse width can be measured. If the instrument allows the radiofrequency power to be adjusted, then the ninety degree pulse width can be set to an appropriate power level which may be safely used for $^{1}$H decoupling during $^{13}$C NMR data acquisition. The $^{1}$H MAS spectrum of a rotor of adamantane spinning at 5 kHz is shown in the top spectrum C of Figure 9.

If the $^{1}$H spectrum is acquired on a static sample (as shown in the bottom spectrum A of Figure 9), the proton resonance has a full width at half maximum (FWHM) of about 12,500 Hz. The line width results primarily from $^{1}$H-$^{1}$H homonuclear dipolar interactions. If the sample is spun slowly, at 500 Hz as shown in the middle spectrum B of Figure 9, no appreciable line narrowing is observed However, if the rotor is spun at 5,000 Hz, the line width narrows to a FWHM around 900 Hz. This homonuclear dipolar broadening is an example of what the NMR literature refers to as a homogeneous (16,17) interaction. As a working definition of a homogeneous interaction, one must spin the sample on the order of the line width before an appreciable narrowing of the resonance occurs. If the sample is spun slowly, then no appreciable line narrowing is observed. This is usually the result of a many-body interaction in which the interaction is distributed over all the spins. The observation of the $^{13}$C spectrum, on the other hand, (vide infra) demonstrates an inhomogeneous (16,17) interaction.

Additionally, it should be pointed out that $^{1}$H rotational echoes in the time domain can also be seen for adamantane when spinning at 5,000 Hz (Figure 10). However, these rotational echoes from the homonuclear dipolar interaction remain relatively broad by comparison with echoes observed for $^{79}$Br when spinning KBr at the magic angle.

Rotational echoes correspond to spinning sidebands in the frequency-domain $^{1}H$ spectrum.

In summary, by observing the $^{1}H$ spectrum of adamantane the proton resonance frequency of adamantane can be determined and can be used as the frequency for $^{1}H$ decoupling. In addition, the $^{1}H$ ninety degree pulse width can be measured or set to a desired value if the spectrometer hardware allows control of the radiofrequency power.

## $^{13}C$ MAS

The third step is to observe the $^{13}C$ MAS spectrum of adamantane. Once again the purpose is twofold. First, the resonance frequency and appropriate spectral width for $^{13}C$ can be determined. In addition, the referencing of the $^{13}C$ chemical shift can be assigned. Second, the $^{13}C$ ninety degree pulse width can be measured (or set to a specific value if the hardware allows).

The experimental parameters for $^{13}C$ NMR observation must be set. An initial spectral width of 100,000 or 125,000 Hz can be used. This spectral width can later be optimized to cover a specific range. An acquisition time of 30 to 60 ms should be sufficient. The pulse program used is once again a single pulse followed by data acquisition. A recycle delay of 3 seconds can be used. The $^{13}C$ MAS spectrum adamantane in a rotor spinning at approximately 3 kHz may be seen in one scan or a few scans on most spectrometers. While slowing the rotation speed down to 3 kHz is not necessary at this point for $^{13}C$ MAS, it will be useful for the $^{13}C$ CP/MAS experiment on adamantane for reasons discussed in the next section. The observation frequency and spectral width can be set to cover a range from 300 ppm to -50 ppm when the upfield methine peak of adamantane is set to 29.46 ppm (18). (The topics of chemical shift referencing and choice of spectral width are addressed in more detail below.) An improvement in $^{13}C$ sensitivity can be achieved by using high power $^{1}H$ decoupling (19) during the acquisition of the data. At this point, the ninety degree pulse width for $^{13}C$ can be measured and adjusted (assuming the necessary spectrometer hardware is available) to the same numerical value as that used for protons. The improvement in the $^{13}C$ sensitivity with the addition of $^{1}H$ decoupling can be seen by comparing the middle spectrum (B) of Figure 11 to that of the bottom spectrum (A) in the same figure. It should be noted that the application of $^{1}H$ decoupling causes the time domain signal to last significantly longer than the 60 ms acquisition time. To avoid oscillation in the frequency domain from truncation of the signal, exponential line broadening may be applied to the time domain signal. Very long data acquisition times with high-power $^{1}H$ decoupling may damage the probe.

The question may be raised of how single frequency continuous wave $^{1}H$ decoupling can be used in solids yet solution-state $^{13}C$ requires broadband decoupling. The homonuclear dipolar broadening of the protons is a homogeneous interaction. As a result, the irradiation of a narrow range of frequencies results, through spin diffusion, in an effect at all protons, thus saturating the entire line shape. By contrast, a "hole is burned" in an inhomogeneous interaction, as only that narrow range frequencies is saturated. If no mechanism for spin diffusion is present, then the saturation does not spread throughout the spectrum. This is more generally the case in liquids, and one must irradiate across a wide band to produce effective decoupling in liquids.

## $^{13}$C CP/MAS

Adjusting the ninety degree pulse widths of both the protons and carbons to the same numerical value insures that one is at, or at least very close to, the necessary Hartmann-Hahn (20) matching condition for the $^{1}$H-$^{13}$C cross-polarization. The Hartmann-Hahn condition requires

$$\omega_{1Hrf} = \omega_{13Crf}$$

where $\omega = \gamma H_1$, with $H_1$ being the radiofrequency magnetic field strengths for the nuclei and with $\gamma$ being the magnetogyric ratio for each nucleus. The flip angle $\theta$ is simply $\omega t_p$, where $t_p$ is the pulse width. As a result, making the ninety degree pulse widths for both $^{1}$H and $^{13}$C the same allows one to match the Hartmann-Hahn condition.

The final step is the $^{1}$H-$^{13}$C cross-polarization/MAS experiment. With a rotor full of adamantane spinning at approximately 3 kHz and with the $^{1}$H and $^{13}$C power levels adjusted to give the same ninety degree pulse width, only the pulse program needs to be changed to that for cross-polarization. The cross-polarization pulse sequence, shown in Figure 12, begins with a $^{1}$H decoupler ninety degree pulse. The phases of the radiofrequency pulses are defined relative to the axes of the rotating frames of the nuclei. If the $^{1}$H ninety degree decoupler pulse has a radiofrequency phase of X, then the proton magnetization is along the Y axis in the rotating frame. The phase of the $^{1}$H decoupler is then switched to the Y phase in order to lock the magnetization along this axis while the $^{13}$C radiofrequency pulse is turned on simultaneously. During this time (typically ranging from 0.5 ms to 10 ms), the polarization is transferred from the protons to the carbons. Finally, the $^{13}$C radiofrequency is turned off to allow acquisition of the $^{13}$C data while the $^{1}$H decoupler remains on during the acquisition.

The $^{13}$C CP/MAS spectrum for admantane, acquired with a Hartmann-Hahn contact time of 5 ms, is shown in the top spectrum (C) of Figure 11. Previous adjustment of the radiofrequency power levels such that the ninety degree pulses for both protons and carbons are the same should be sufficiently close to the Hartmann-Hahn match that a cross-polarization signal is obtained. Of course the cross-polarization signal can be optimized by varying the $^{13}$C radiofrequency power to obtain the largest signal intensity. One reason to optimize the $^{13}$C sensitivity with the $^{13}$C radiofrequency power (as opposed to the $^{1}$H power) is that the $^{1}$H power is still left on after the Hartman-Hahn match to provide the $^{1}$H decoupling. Application of too much radiofrequency power may cause arcing in the probe. If arcing is observed during data acquisition (appearing as spikes of noise or noise completely clipped by the analog-to-digital converter), this is on the $^{1}$H channel since this is the only radiofrequency on at that time. If the signal completely disappears with only normal noise, the arcing is probably on the $^{13}$C channel.

The performance specifications for a particular probe should be provided with the probe. For a commercial probe these should be readily available. For homemade probes, acquiring this information may pose a challenge (or require a research project). Usually the power specification is given as a pulse width for a ninety degree pulse or as a decoupling field expressed in kHz along with the maximum time it can safely be used. For direct observation of a nucleus, the ninety degree pulse may be measured directly by nulling the signal with a 180 degree or 360 degree pulse and appropriately dividing the

result to obtain the ninety. One caveat arises when the rise and fall times of the pulse are significant fractions of the total pulse width. In this case, one may find that the 360 degree pulse width is not simply two times that of the 180 degree pulse.

The decoupling field is expressed as the inverse of the 360 degree pulse width. As a specific example, the CP/MAS probe with a 4 mm outside diameter rotor used for the acquisition of data in this article was specified in 1999 to have a 3.5 μs cross-polarization ninety degree pulse with a maximum $^{1}H$ radiofrequency decoupling field of 100 kHz which could be used for a maximum decoupling time of 50 ms. The $^{1}H$ decoupling field of 100 kHz corresponds to a $^{1}H$ ninety degree pulse width of 2.5 μs. Exceeding the specifications for the probe may result in arcing and may permanently damage the probe.

In the usual cross-polarization pulse sequence shown in Figure 12, the $^{1}H$ ninety degree decoupler pulse can be measured by increasing the $^{1}H$ decoupler pulse to a 180 degree pulse and observing the observation of a null $^{13}C$ signal in the CP/MAS experiment. The $^{13}C$ ninety degree pulse width can be directly measured by use of the modification shown in Figure 13. This sequence begins with the usual cross-polarization followed by a $^{13}C$ pulse, shifted in phase from the cross-polarization by ninety degrees. Setting this pulse width to zero (or a very small flip angle) yields the usual $^{13}C$ CP/MAS spectrum. However, when this pulse width is set to 90 degrees, the $^{13}C$ CP/MAS spectrum is nulled.

The mechanism of cross-polarization is usually explained in terms of either thermodynamics or quantum mechanics (5,7). First consider the thermodynamic model. In thermodynamic terms, one can think of lowering the temperature as a way to increase order. For example, consider a gas as a disordered arrangement of atoms or molecules completely filling the volume available to it. As one lowers the temperature, the gas condenses into a liquid with an increase in local order. Finally, as one lowers the temperature enough, the liquid freezes into a solid. The atoms or molecules become even more ordered as they now occupy lattice positions. That is, the general concept is that order is increased as the temperature is lowered.

The NMR experiment begins with the magnetization at equilibrium ($M_0$) aligned with the static magnetic field (which defines the Z axis). There is no net magnetization in the X-Y plane. In terms of statistical mechanics, this is often referred to as the random phase approximation. In terms of quantum mechanics, one is not allowed by the uncertainty principle to measure all three components of the angular momentum simultaneously. However, the NMR experiment is made by measuring the projection of the magnetization in the X-Y plane. So, in terms of NMR, initially there is no magnetization (order) in the X-Y plane for both the protons and carbons. It is possible to think of the proton and carbon spin systems as being hot. The spin temperature of the protons can be lowered by applying a ninety degree pulse and spin locking the proton magnetization to create order in the X-Y plane. Rigorously, though, the concept of spin temperature (5,7) is given relative to a magnetic field. In the high temperature approximation, in which the thermal energy given by the product of the Boltzmann constant with the temperature is greater than the separation of the magnetic energy levels, the magnetization $M_0$ displays a Curie law behavior. That is, the magnetization is directly proportional to the magnetic field strength and inversely proportional to the temperature. This high temperature approximation is typically valid for spin ½ nuclei above 4 K. Since the initial proton magnetization $M_0$ at equilibrium along the large static laboratory magnetic field is the

same magnetization which is spin locked after the ninety degree pulse, the much smaller magnetic field of the spin lock radiofrequency pulse requires a much lower spin temperature due to the Curie law. Physically it is the spin locking of the proton magnetization which lowers the spin temperature of the protons. Spin locking after the ninety degree pulse provides proton magnetization (order) in the X-Y plane with the protons at a lower temperature. Of course, the carbons are hot and have no order in the X-Y plane. The thermal contact between the cold protons and hot carbons is made by applying a simultaneous radiofrequency pulse to the carbon spin system while the protons are spin locked. It is necessary for these simultaneous radiofrequency pulses on both spin systems to match the Hartman-Hahn condition. This thermal contact is made through the dipolar interaction, with the applied radiofrequency allowing normally forbidden transitions to occur. As the protons warm, the carbons cool, generating $^{13}C$ magnetization in the X-Y plane. The $^{1}H$ decoupler may be left on as the $^{13}C$ signal is acquired.

In terms of a quantum mechanical description, the energy levels of a spin are given by the dot product of the magnetic moment with the magnetic field. The magnetogyric ratios of the protons and carbons are constants. The static magnetic field in the laboratory does not permit the energy levels of nuclei with differing magnetogyric ratios to be the same. However, magnetic fields in the rotating frame arise from the applied radiofrequency pulses. By matching the Hartmann-Hahn condition, the magnetic fields from the radiofrequency pulses are of such a magnitude that the protons and carbons have a common energy level scheme. That is, the energy levels for the protons and carbons are matched in the rotating frames of the two different nuclei. Again, the normally forbidden transitions of the dipolar interaction can allow the two spin systems to exchange energy.

These models require a dipolar interaction for the cross-polarization from the protons to the carbons to occur. However, the description of each model is for cross-polarization in a manner independent of the magic angle spin rate. A difficulty can arise since magic angle spinning is able to average out the dipolar interaction. For this reason the Hartman-Hahn match on adamantane is adjusted with a relatively slow spinning speed of 3 kHz. While adamantane is a solid at ambient temperature, it is "a classic example of the 'typical' plastic crystal" (6). There is significant molecular motion at ambient temperature (as the molecules themselves are almost like small spheres). As a result, one does not have to spin very rapidly at the magic angle to average out the heteronuclear dipolar interaction and lose the ability to cross-polarize through that particular interaction.

As mentioned earlier, one can optimize the Hartmann-Hahn match by varying the $^{13}C$ radiofrequency power to find the largest signal. This is shown in Figure 14 in which the top trace (C) shows the upfield methine resonance of a static sample of adamantane plotted repeatedly as the $^{13}C$ amplifier gain is decreased in twenty steps of 0.25 dB. The modulation of the signal amplitude from even the modest spinning speed of 3 kHz upon the $^{1}H$-$^{13}C$ heteronuclear interaction is readily apparent in (B). However, a sample more representative of a real solid does not show nearly as sharp a match nor does it show such a modulation. For example, the methylene resonance of a common polymorph of glycine, $\alpha$-glycine ($C_2H_5NO_2$) (21), as a function of the same power changes remains almost constant, as shown in the bottom trace (A) of Figure 14.

Once the experiment has been set up and the $^{13}C$ chemical shift calibrated, samples of interest may be run. For example, the $^{13}C$ CP/MAS spectrum of α-glycine with a sample rotation speed of 10 kHz is shown in the bottom spectrum (A) of Figure 15. At high spinning speeds, the isotropic peaks for the carbonyl and methylene resonances are observed along with spinning sidebands from carbonyl resonance.

A close examination at the methylene resonance shows the dipolar coupling (22-25) of the $^{14}N$ with its quadrupole moment to the $^{13}C$, as shown in Figure 16. In essence, when the $^{14}N$ nuclei have electric quadrupole interactions comparable to the size of their Zeeman interactions, the quadrupolar interaction mixes the pure Zeeman states of the quadrupolar nucleus. As a result of this mixing, there are now new terms in the dipolar coupling Hamiltonian. Since the angular dependence is no longer the familiar second order Legendre polynomial ($3\cos^2\theta - 1$), the interaction can not be averaged by magic angle spinning. At lower fields this coupling can be useful for identifying which carbon atoms are adjacent to nitrogen atoms. At higher field strengths or with $^{15}N$ labelled materials, this coupling will not be seen.

Figure 15 shows the $^{13}C$ CP/MAS spectra of α-glycine acquired as a function of spinning speed. At high spinning speeds, the isotropic resonances and a few spinning sidebands, as discussed above, are seen in spectra (A) and (B). However, the rotor can be spun at slow rotation speeds of 1 kHz or less and still yield very narrow lines. Of course, many more spinning sidebands are observed under these conditions. Finally, the spectrum from the static sample can be acquired. By comparing the static spectrum (D) with that of the slow spinning at 500 Hz (C) in Figure 15, one sees that the spinning sidebands arise from the chemical shift anisotropy. Indeed, one can analyze the spinning sidebands with the Herzfeld-Berger (26) method to obtain the principal values of the chemical shift anisotropy. Software for this analysis (and many other solid state simulations) is available online from the research group of Dominique Massiot (27). Additionally, it should be pointed out that when an interaction is narrowed even when spinning slowly compared to the line width, the interaction is referred to as inhomogeneous. In this case, the actual line widths are very narrow though there are a substantial number of spinning sidebands.

This may be a good point to offer comments regarding the referencing of $^{13}C$ chemical shifts and choice of spectral widths. The use of an external standard for referencing solid-state $^{13}C$ MAS has been studied over the years (28-33). More recently, Morcombe and Zilm (18) have shown that adamantane can easily be used to reference $^{13}C$ MAS spectra externally with a precision of +/- 0.03 ppm. As for the choice of an appropriate spectral width, the spectra of α-glycine as a function of spinning speed show that a spectral width from 300 ppm to -50 ppm should allow the $^{13}C$ data acquisition as a general survey spectrum of most compounds without folding or aliasing any of the spinning sidebands in the spectrum. Of course, when both the chemical shifts and anisotropies are known, the spectral width can be optimized for a particular compound. In solid-state NMR, the data acquisition time (which can be independently adjusted by varying the number of data points acquired) is usually a more important parameter than the spectral width due to the generally higher power used for $^{1}H$ decoupling as compared with solution NMR. For many compounds in the solid state, acquisition times of 30 to 100 ms are sufficient. Only unusually narrow resonances, such as those found for

adamantane, require longer acquisition times in order to avoid truncating the time domain signal.

The unusually narrow resonance of adamantane makes it suitable for shimming a MAS probe. The molecular motion of adamantane is such that a relatively low $^{1}H$ decoupling power is required to remove the $^{1}H$-$^{13}C$ dipolar interaction. This allows one to match the Hartman-Hahn condition with a $^{1}H$ power level that gives a much longer ninety degree pulse. The lower $^{1}H$ power allows much longer acquisition times (with $^{1}H$ decoupling) so that the full decay of the adamantane signal can be acquired without damaging the probe. The amount of power that can be used without damaging the probe is probe-dependent and should be provided by the maker of the probe, as discussed above. Usually at lower magnetic field strengths with proton resonances at 200 or 300 MHz, one may be able to shim the adamantane resonances to a FWHM of two or three Hz. With a well shimmed probe, the $^{13}C$-$^{13}C$ satellites with a scalar coupling of 31.6 Hz may even be resolved. Such a spectrum is shown in Figure 17. At higher field strengths such narrow lines may be more difficult to achieve. To measure lines as narrow as a couple of Hz requires acquisition times on the order of one-half to one second. The $^{1}H$ decoupling power must be sufficiently low so as not to damage the probe while still providing decoupling.

While single frequency continuous wave $^{1}H$ decoupling works, the two pulse phase modulation (TPPM) (34) decoupling scheme offers significant improvement for a strongly coupled homogeneous spin system undergoing MAS at spinning speeds up to 12 kHz. As a result, this decoupling sequence is often used in practice for the acquisition of data from samples of interest. The decoupling consists of the application of $^{1}H$ radiofrequency pulses alternating between two phases separated by an angle $\phi$. Such a sequence can be optimized as a function of the decoupler transmitter frequency, the phase angle, and the pulse width. A phase angle of 30 degrees and a pulse width just short of a 180 degree pulse usually work well. The optimization of the TTPM sequence as a function of the $^{1}H$ pulse width is shown in Figure 18. The methylene peak of $\alpha$-glycine is plotted twenty times as the pulse width is incremented from 5.7 $\mu$s in steps of 0.1 $\mu$s.

## SUMMARY

In conclusion, the first step in initially setting up a $^{1}H$-$^{13}C$ CP/MAS experiment is observation of $^{79}Br$ MAS in KBr to check the angle setting of the probe and to set the magnetic field to a specific value. In future experiments, this frequency can then be used as a solid-state NMR "lock" to set the magnetic field reproducibly to the same value each time.

The second step is to observe the protons of adamantane. This allows one to determine the resonance frequency of the protons and to adjust the $^{1}H$ power for the appropriate ninety degree pulse.

The third step is to measure the $^{13}C$ MAS (usually with $^{1}H$ decoupling) spectrum of adamantane. This allows one to determine the $^{13}C$ frequency, set the appropriate spectral window, and reference the chemical shifts. In addition one can also adjust the $^{13}C$ ninety degree pulse width so that one is already at or near the Hartman-Hahn match.

Finally, one can run the $^{1}H$-$^{13}C$ CP/MAS experiment on adamantane. Then one is ready to proceed with samples of interest.

## ACKNOWLEDGEMENT

The author would like to thank Dr. Detlef Mueller of Bruker BioSpin GmbH for the photos of the probe and permission to use them. The author would also like to thank Ms. Susie Huang for assistance in the preparation of the figures.

## REFERENCES

1. Schaefer J, Stejskal EO. Carbon-13 Nuclear Magnetic Resonance of Polymers Spinning at the Magic Angle. J Am Chem Soc 1976; 98(4): 1031-1032.

2. Pines A, Gibby MG, Waugh JS. Proton-Enhanced Nuclear Induction Spectroscopy. A Method for High Resolution NMR of Dilute Spins in Solids. J Chem Phys 1972; 56(4): 1776-1777.

3. Andrew ER, Bradbury A, Eades RG. Nuclear Magnetic Resonance Spectra from a Crystal rotated at High Speed. Nature 1958; 182:1659.

Andrew ER, Bradbury A, Eades RG. Removal of Dipolar Broadening of Nuclear Magnetic Resonance Spectra of Solids by Specimen Rotation. Nature 1959: 183:1802-1803.

4. Lowe IJ. Free Induction Decays Of Rotating Solids. Phys Rev Letters 1959: 2(7):285-287.

5. Mehring M. High Resolution NMR Spectroscopy in Solids (NMR: Basic Principles and Progress: Vol. 11). Berlin: Springer: 1976.

6. Fyfe CA. Solid State NMR for Chemists. Guelph, Ontairo, Canada: C. F. C. Press: 1983.

7. Schlichter CP. Principles of Magnetic Resonance (Second Edition). Berlin: Springer: 1978.

8. Olivieri, AO. Illustrating NMR Cross-Polarization (CP) with a Microcomputer. Concepts Magn Reson 1998: 10(6): 343-354.

9. Bain AD, Dumont RS. Introduction to Floquet Theory: The Calculation of Spinning Sieband Intensities in Magic-Angle Spinning NMR. Concepts Magn Reson 2001; 13(3): 159-170.

10. Laws DL, Bitter H-ML, Jerschow A. Solid-State NMR Spectroscopic Methods in Chemistry. Angew Chem Int Ed 2002; 41: 3097-3129.

11. Voelkel R. High-Resolution Solid-State $^{13}$C-NMR Spectroscopy of Polymers. Angew Chem Int Ed Engl 1988: 27: 1468-1483.

12. Aliev AE, Law RV. Solid-State NMR Spectroscopy. In: Webb GA, editor. A Specialist Periodical Report Nuclear Magnetic Resonance; Cambridge: The Royal Society of Chemistry; 2003. p238-291.

13. Frye JS, Maciel GE. Setting the Magic Angle Using a Quadrupolar Nuclide. J Magn Reson 1982; 48: 125-131.

14. Meisalo V, Inkinen O. An X-ray Diffraction Analysis of Potassium Bromide. Acta Cryst 1967; 22: 58-65.

15. Brevard C, Granger P. Handbook of High Resolution Multinuclear NMR. New York: John Wiley and Sons; 1981.

16. Maricq MM, Waugh, JS. NMR in rotating solids. J Chem Phys 1979; 70(7): 3300-3316.

17. Portis, AM. Electronic Structure of F Centers: Saturation of the Electron Spin Resonance. Phy Rev 1953; 91(5): 1071-1078.

18. Morcombe CR, Zilm KW. Chemical shift referencing in MAS solid state NMR. J Magn Reson 2003: 162: 479-486.

19. Sarles LR, Cotts RM. Double Nuclear Magnetic Resonance and the Dipole Interaction in Solids. Phys Rev 1958; 111: 853.

20. Hartmann SR, Hahn EL. Nuclear Double Resonance in the Rotating Frame. Phys Rev 1962: 128(5): 2042-2053.

21. Potrzebowski MJ, Tekely P, Dusausoy Y. Comment to $^{13}$C-NMR studies of $\alpha$ and $\gamma$ polymorphs of glycine. Solid State NMR 1998; 11: 253-257.

22. Stoll ME, Vaughan RW, Saillant RB, Cole T. $^{13}$C chemical shift tensor in $K_2Pt(CN)_4Br_{0.3}$.3H2O. J Chem Phys 1974; 61(7): 2896-2899.

23. Opella SJ, Frey MH, Cross TA. Detection of Individual Carbon Resonances in Solid Proteins. J Am Chem Soc 1979; 101(19): 5856-5857.

24. Zumbulyadis N, Henrichs PM, Young RH. Quadrupole effects in the magic-angle-spinning spectra of spin-1/2 nuclei. J Chem Phys 1981; 75(4): 1603-1611.

25. Olivieri AC. Quadrupolar Effects in the CPMAS Spectra of Spin-1/2 Nuclei. J Magn Reson 1989; 81: 201-205.

26. Herzfeld J, Berger AE. Sideband Intensities in NMR spectra of samples spinning at the magic angle. J Chem Phys 1980; 73(12): 6021-6030.

27. Massiot D, Fayon F, Capron M, King I, Le Calve S, Alonso B, Durand J-O, Bujoli B, Gan Z, Hoatson G. Modelling one- and two-dimensional solid-state NMR spectra. Mag Reson Chem 2002; 40: 70-76. DMFIT program available at http://crmht-europe.cnrs-orleans.fr. (accessed January 29, 2004).

28. Harris, RK, Becker ED, Cabral De Menezes SM, Goodfellw R, Granger P. NMR Nomenclature. Nuclear Spin Properties and Conventions for Chemical Shifts (IUPAC Recommendations 2001). Pure Appl Chem 2001; 73(11): 1795-1818.

29. Earl WL, VanderHart DL. Measurement of $^{13}C$ Chemical Shifts in Solids. J Magn Reson 1982; 48: 35-54.

30. VanderHart DL. Field-dependent C-13 chemical shifts in solids: A second-order dipolar perturbation. J Chem Phys 1986; 84(3): 1196-1205.

31. Hayashi S, Hayamizu K. Shift References in High-Resolution Solid-State NMR. Bull Chem Soc Jpn 1989; 62: 2429-2430.

32. Hayashi S, Hayamizu K. Chemical Shift Standards in High-Resolution Solid-State NMR (1) $^{13}C$, $^{29}Si$, and $^{1}H$ Nuclei. Bull Chem Soc Jpn 1991; 64(2): 685-687.

33. Hayashi S, Hayamizu K. Chemical Shift Standards in High-Resolution Solid-State NMR (2) $^{15}N$ Nuclei. Bull Chem Soc Jpn 1991; 64(2): 688-690.

34. Bennett AE, Rienstra CM, Auger M, Lakshmi KV, Griffin RG. Heteronuclear decoupling in rotating solids. J Chem Phys 1995; 103(16): 6951-6958.

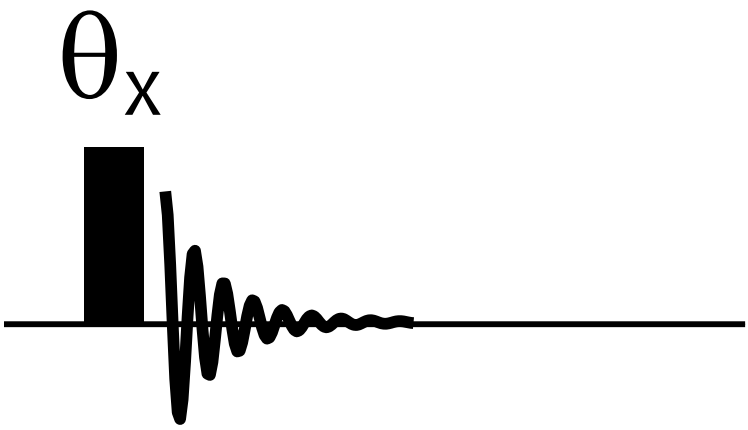


Figure 1: A single radiofrequency pulse of flip angle θ of phase X followed by data acquisition in the time domain. Usually quadrature detection is used to acquire the real (cosine) and imaginary (sine) NMR signals.

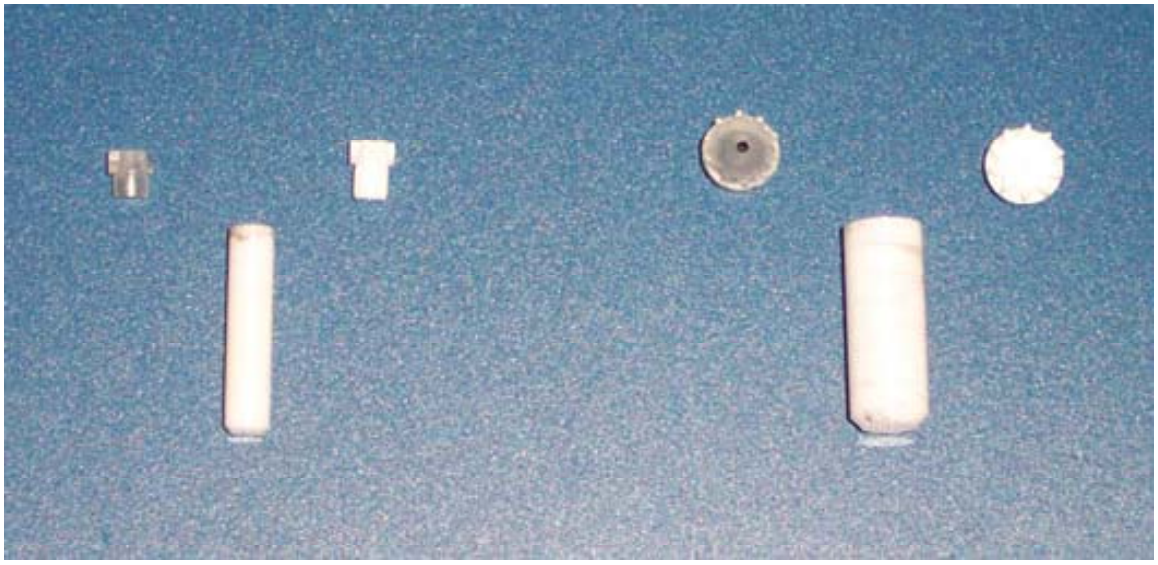

Figure 2: Four and seven millimeter (mm) diameter rotors for MAS. Plastic Kel-F caps may be used at ambient temperatures. Zirconia caps are used for variable temperature experiments.

## NMR-Solenoid coil in an MAS system

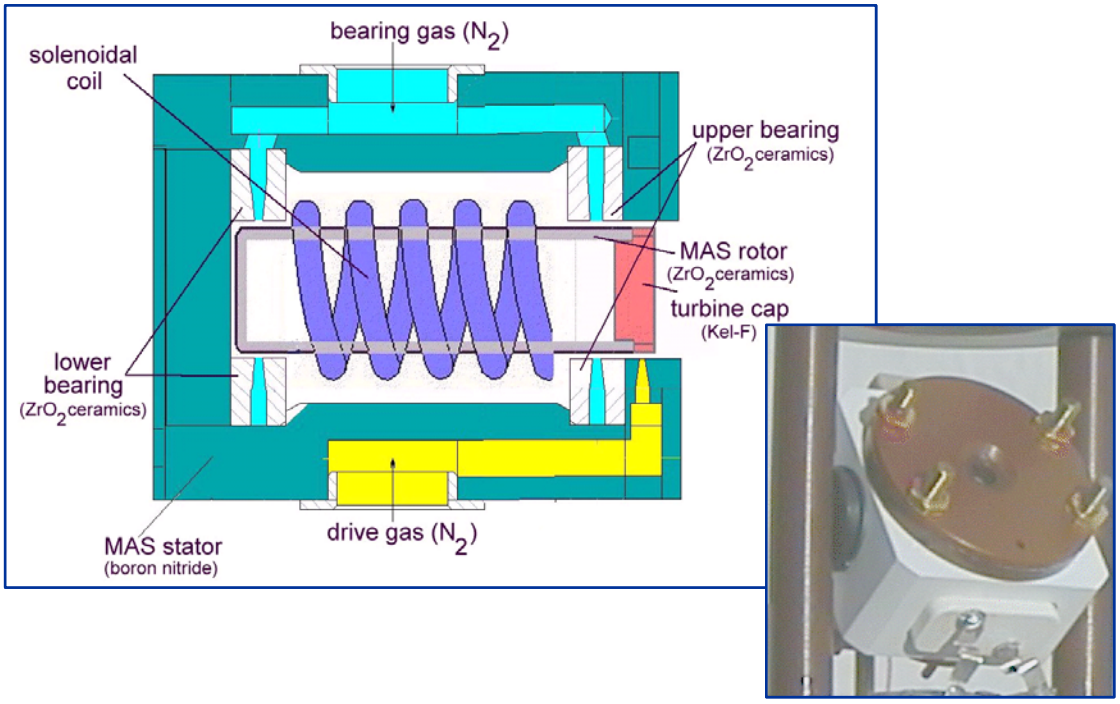


Figure 3: A schematic for a double air bearing stator used for magic angle spinning. A photo of an actual stator is shown in the insert.

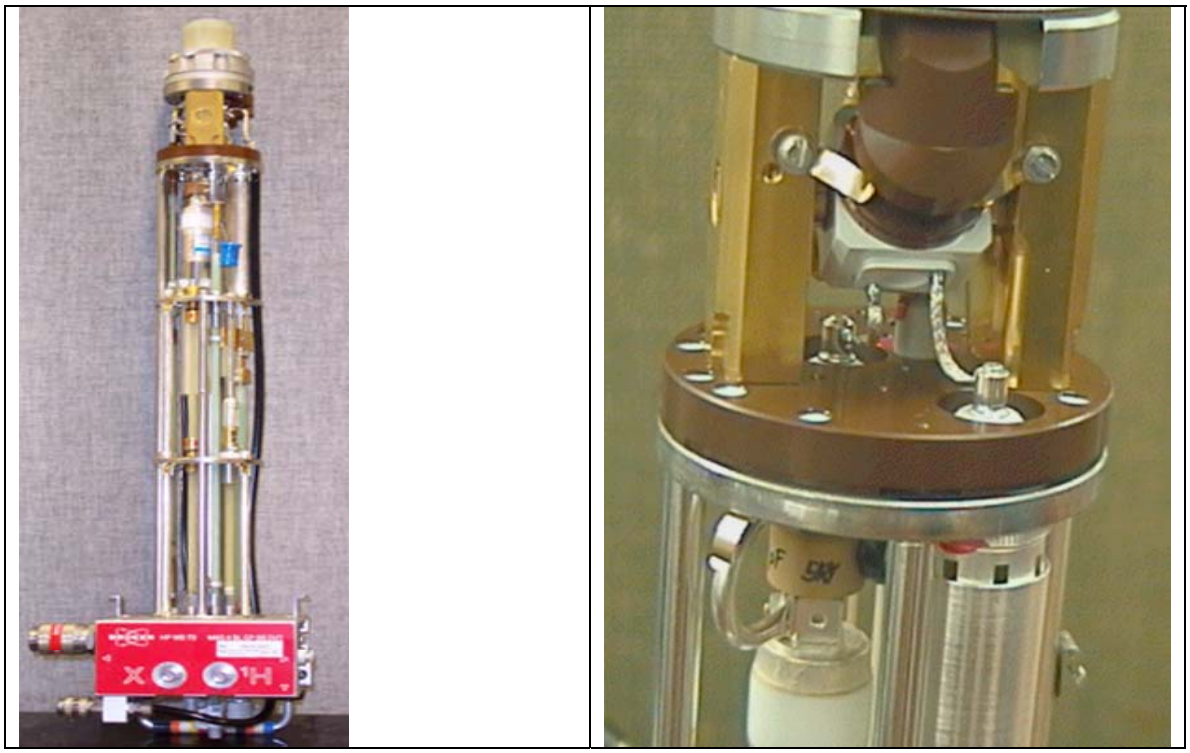

Figure 4: A CP/MAS probe (with cover removed) is shown on the left. A close up showing the stator with the electronics below is shown on the right. Beneath the stator plate is a capacitor with an inductor in parallel to form a $^{1}H$ trap in the $^{13}C$ circuitry. This trap prevents the $^{1}H$ frequency from entering the $^{13}C$ circuitry. The large capacitor beneath the trap provides the frequency tuning for the $^{13}C$.

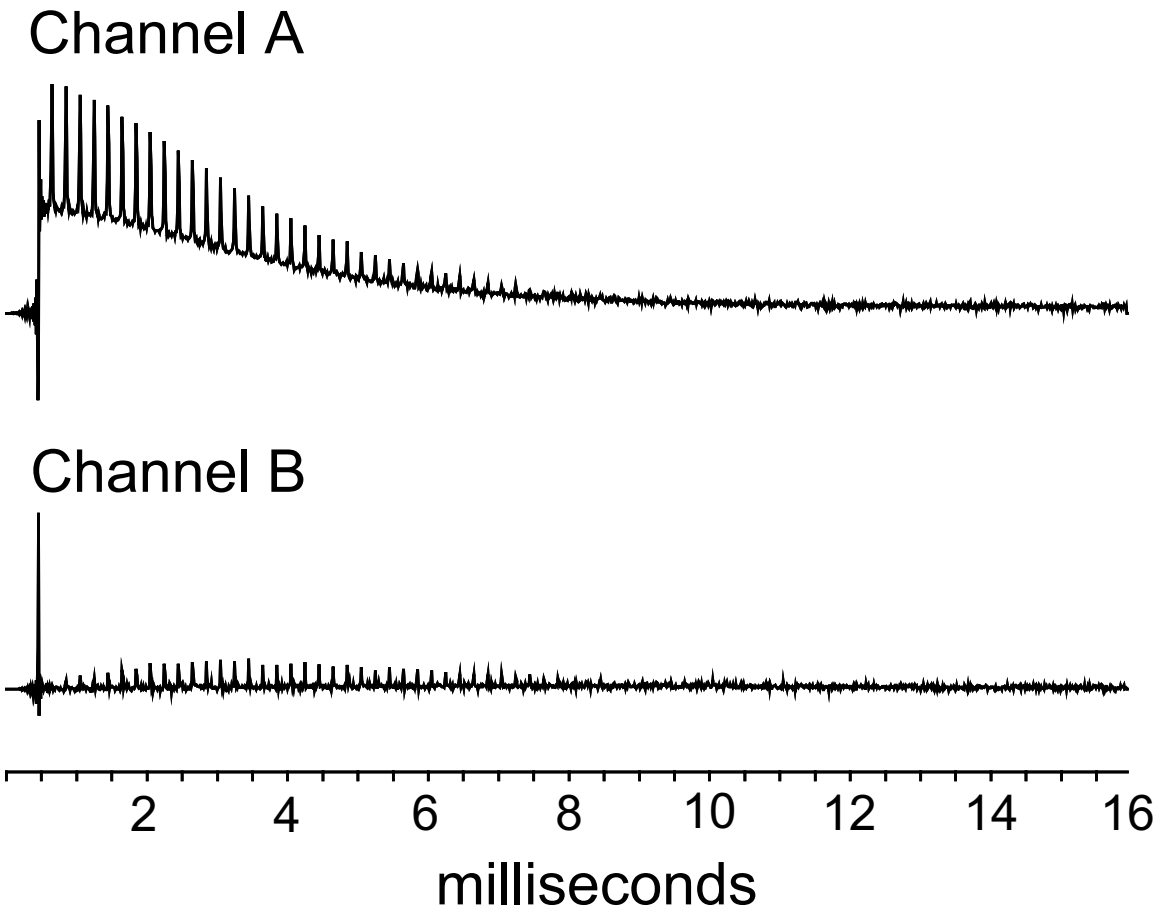


Figure 5: $^{79}$Br MAS time domain signal showing both real (Channel A) and imaginary (Channel B) channels. The real channel corresponds to the cosine and the imaginary corresponds to the sine. The "ringup" at the beginning of each channel is due to the digital filtering used in signal acquisition. The data was acquired at 75.2 MHz ($^{1}$H at 300 MHz) with a single 45 degree pulse (2 μs) and a sample rotation rate of 5,000 Hz. The acquisition time was 16 ms.

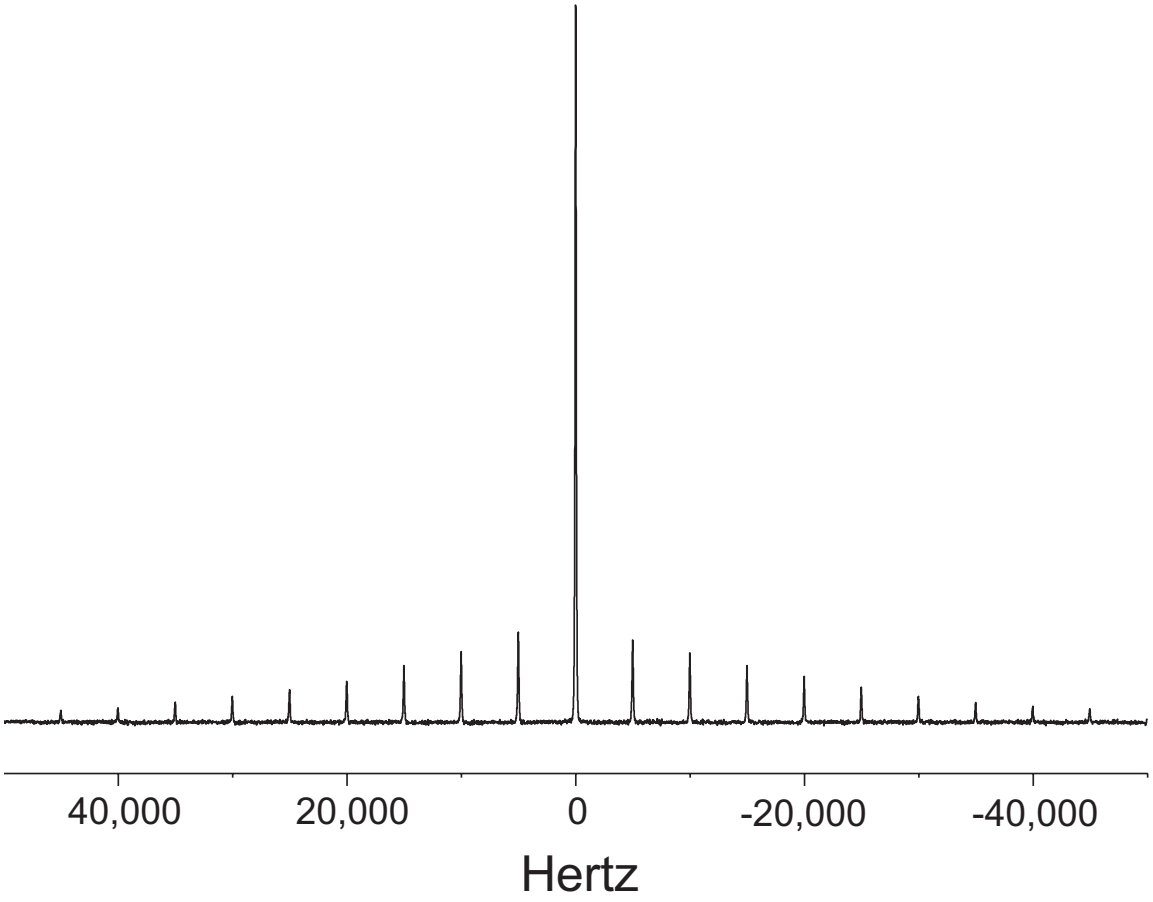


Figure 6: $^{79}$Br MAS spectrum of potassium bromide showing the central transition (arbitrarily assigned to zero ppm) and the spinning sidebands. This is the Fourier transformation of the time domain shown in Figure 5. The growth of magnetization in the imaginary channel as shown in Figure 5 results in a small amplitude roll in the baseline. This baseline roll has been corrected.

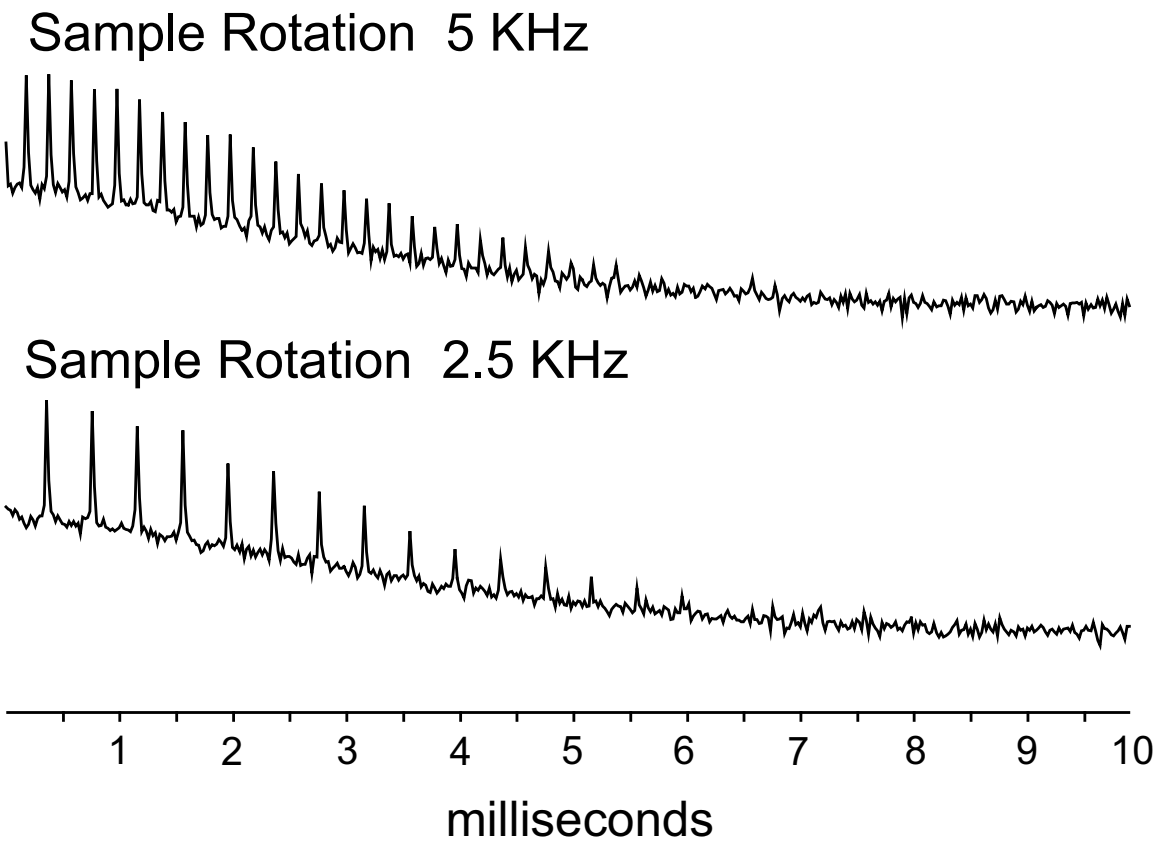


Figure 7: Comparison of the real channels for $^{79}$Br MAS time domain signals of KBr showing rotational echoes with sample rotation rates of 5 kHz (top) and 2.5 kHz (bottom). As the spinning speed is slowed, the echoes are separated further in time as it takes longer for each rotor revolution. The spinning speed may be measured by the time needed for one rotor revolution. This time can be measured from the maximum of one echo to the maximum of the following echo. The acquisition conditions are given in Figure 5.

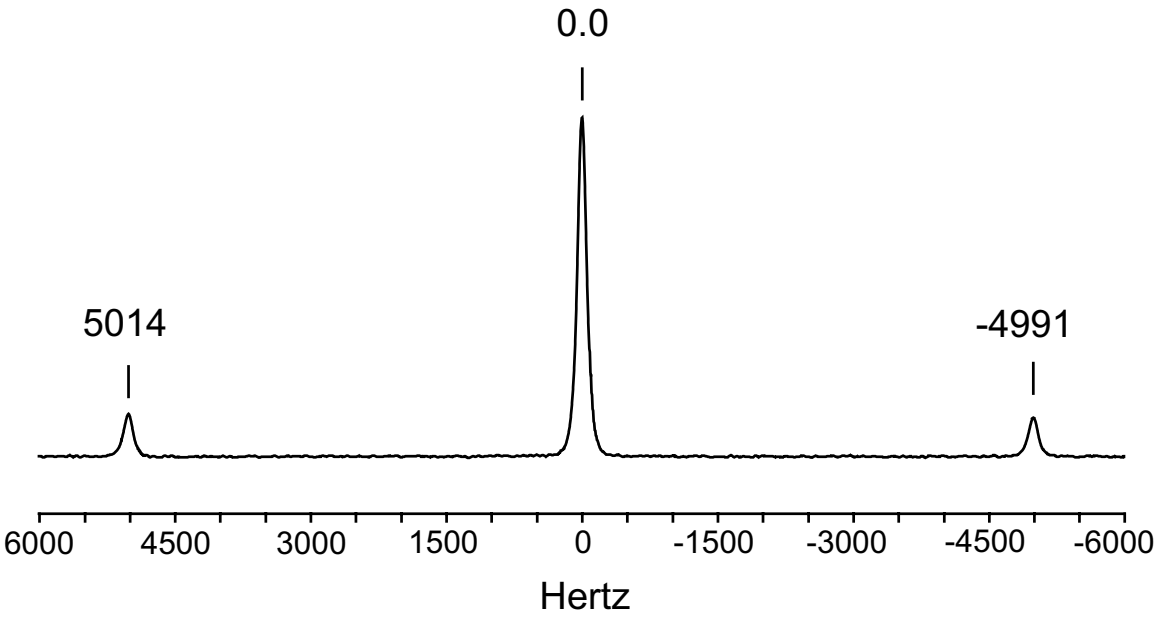


Figure 8: Expanded $^{79}$Br MAS spectrum of potassium bromide showing the central transition (arbitrarily assigned to zero ppm) and the first two spinning sidebands. The spinning sidebands show a small frequency shift relative to the central transition. Acquisition conditions are given in Figure 5.

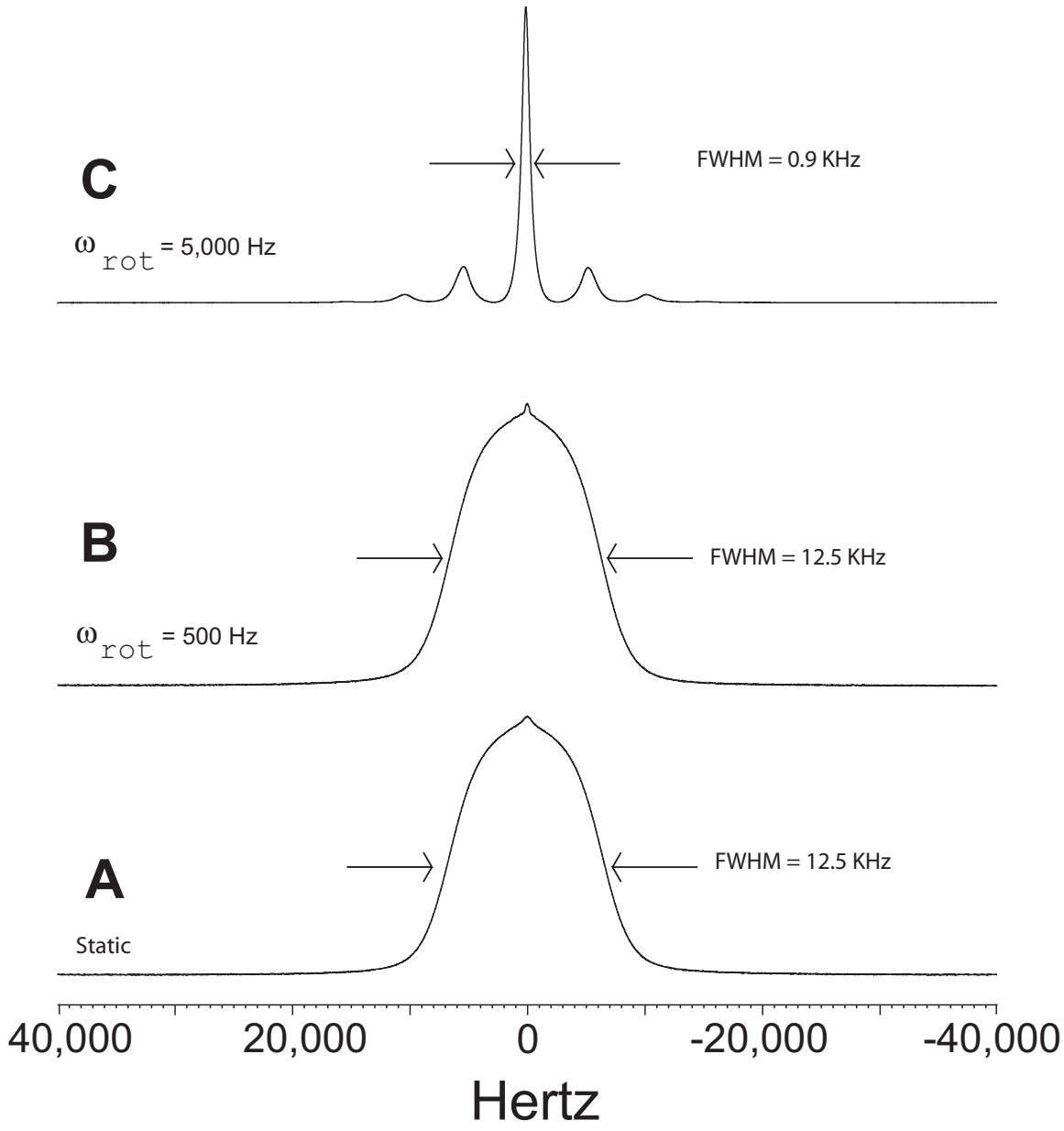


Figure 9: $^{1}H$ spectra of adamantane: static sample (A), 500 Hz MAS (B) and 5,000 Hz MAS (C). The spectra are acquired using a single 90 degree pulse with a spectral width of 100 kHz.

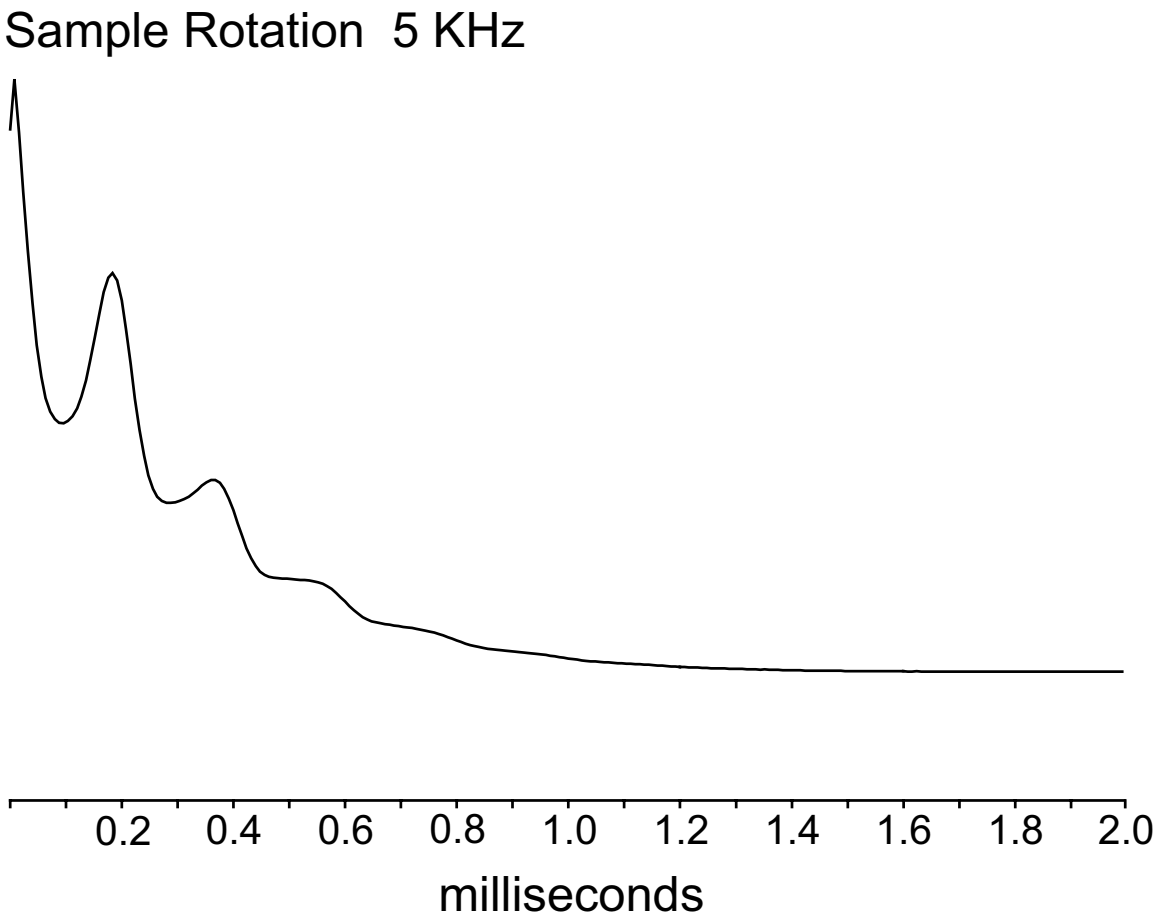


Figure 10: The real channel of the $^{1}H$ MAS time domain signal of adamantane showing rotational echoes. A single 90 degree pulse was used for excitation. The dwell time is 5 μs.

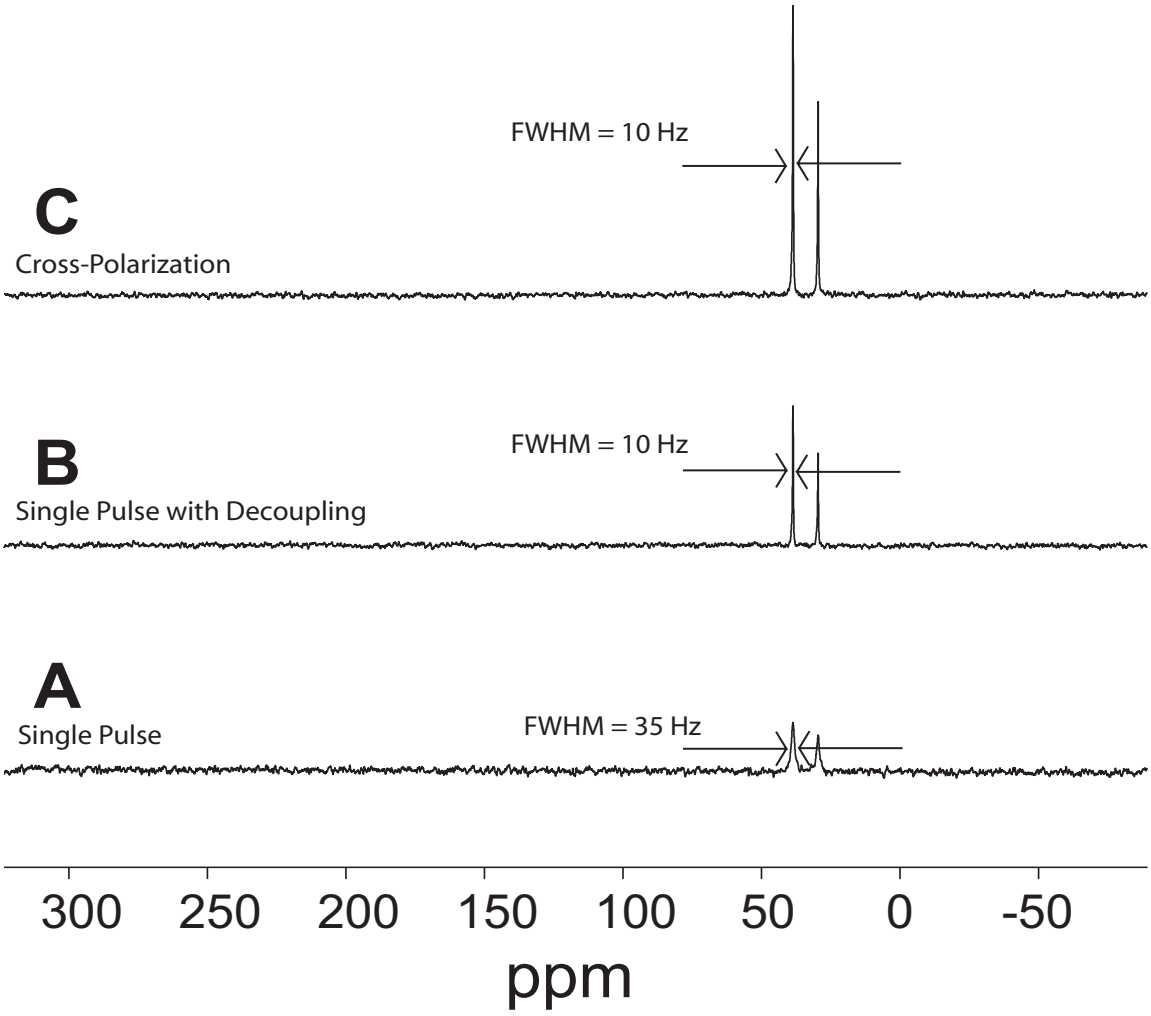


Figure 11: $^{13}C$ MAS NMR spectra of adamantane rotating at 3,000 Hz: single pulse (A), single pulse with $^{1}H$ decoupling (B), and cross-polarization with $^{1}H$ decoupling (C). Spectra A and B were acquired with a single 90 degree pulse of 4.4 μs using a dwell time of 16 μs. In addition, spectrum B has $^{1}H$ decoupling corresponding to a field-strength of 56.8 kHz. The cross-polarization spectrum C had a contact time of 5 ms and the same $^{1}H$ decoupling. All three spectra have the same vertical scaling. The increased resolution (and therefore sensitivity) from $^{1}H$ decoupling in spectrum B relative to A is easily seen. Enhancement from polarization transfer in spectrum C relative to that of spectrum B is seen.

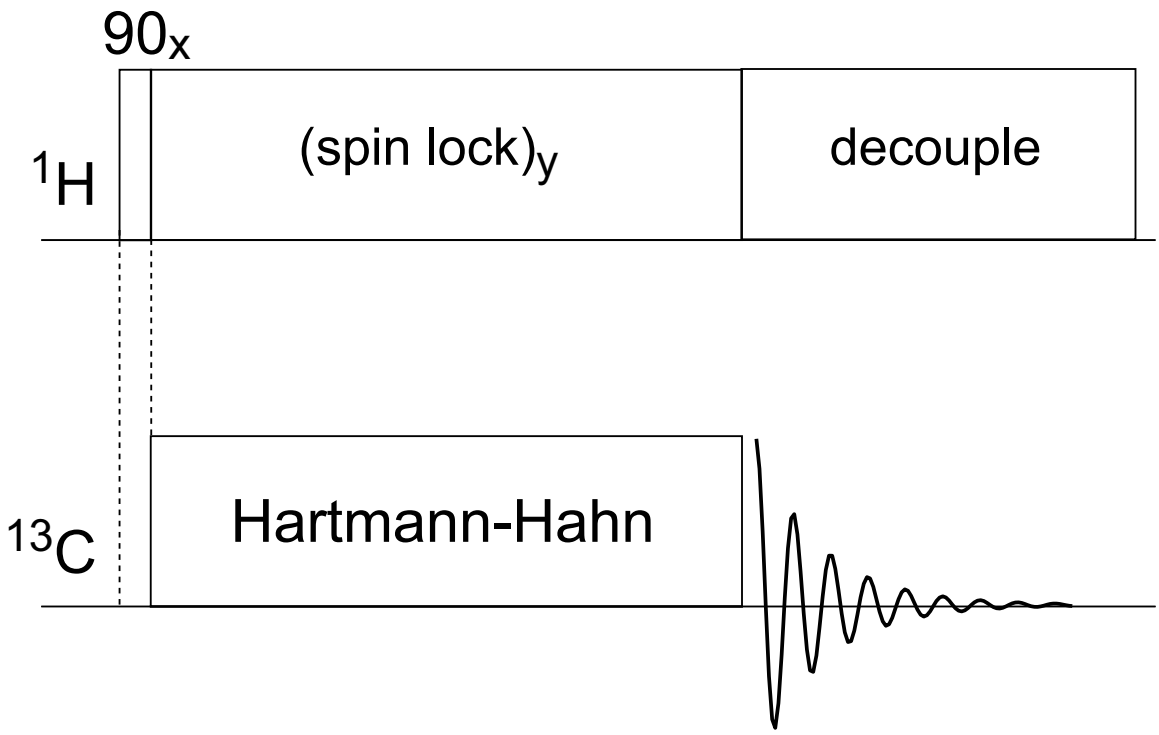


Figure 12: $^{1}H$-$^{13}C$ cross-polarization pulse sequence. The $^{1}H$ ninety degree decoupler pulse brings the proton magnetization into the X-Y plane. The $^{1}H$ radiofrequency is then phase shifted by 90 degrees to spin lock the proton magnetization. Simultaneously the $^{13}C$ radiofrequency is applied matching the Hartmann-Hahn condition. This causes the polarization transfer from the protons to the carbons. When the Hartmann-Hahn (contact) pulse is turned off, the $^{1}H$ radiofrequency is left on during the $^{13}C$ data acquisition in order to provide $^{1}H$ decoupling.

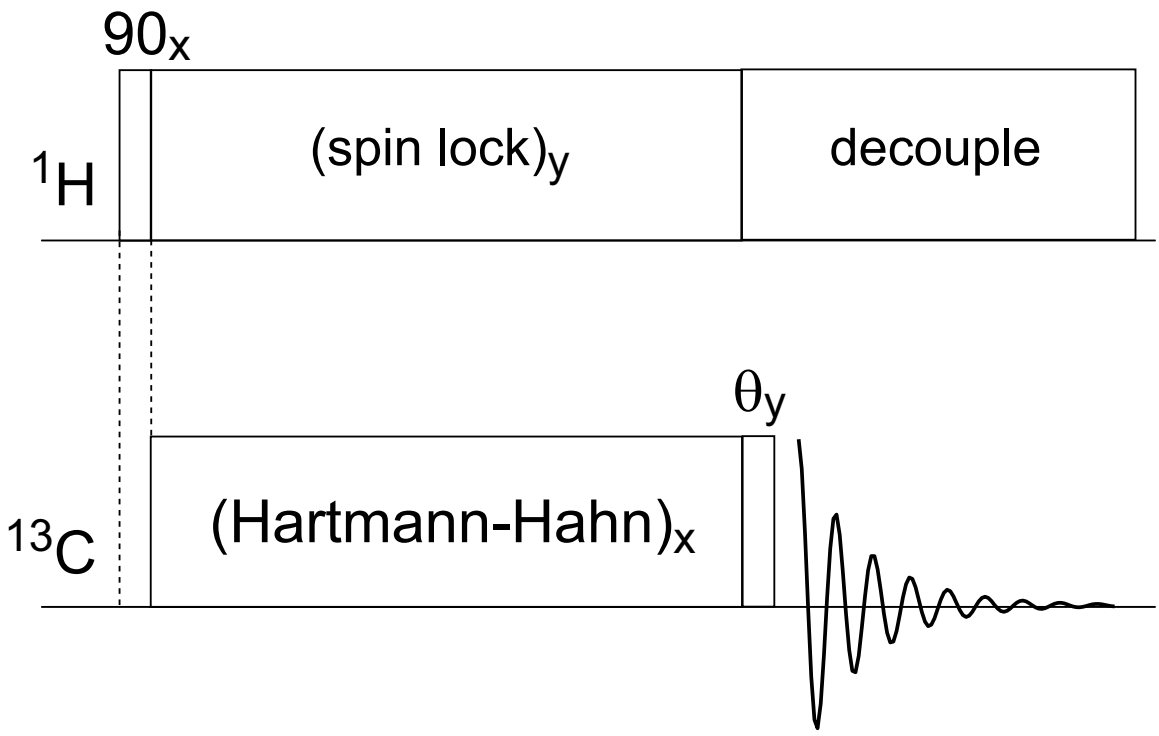


Figure 13: $^{1}H$-$^{13}C$ cross-polarization sequence for measuring the $^{13}C$ ninety degree pulse width. This sequence begins with same cross-polarization sequence described in Figure 12. After the Hartmann-Hahn pulse is turned off for the carbons, then a short $^{13}C$ pulse phase shifted by 90 degrees relative to the Hartmann-Hahn pulse is applied before acquiring the $^{13}C$ data. If this pulse is zero (or at least very short), the usual $^{13}C$ CP signal is obtained. However, when this pulse is a $^{13}C$ 90 degree pulse, the $^{13}C$ CP signal will be nulled.

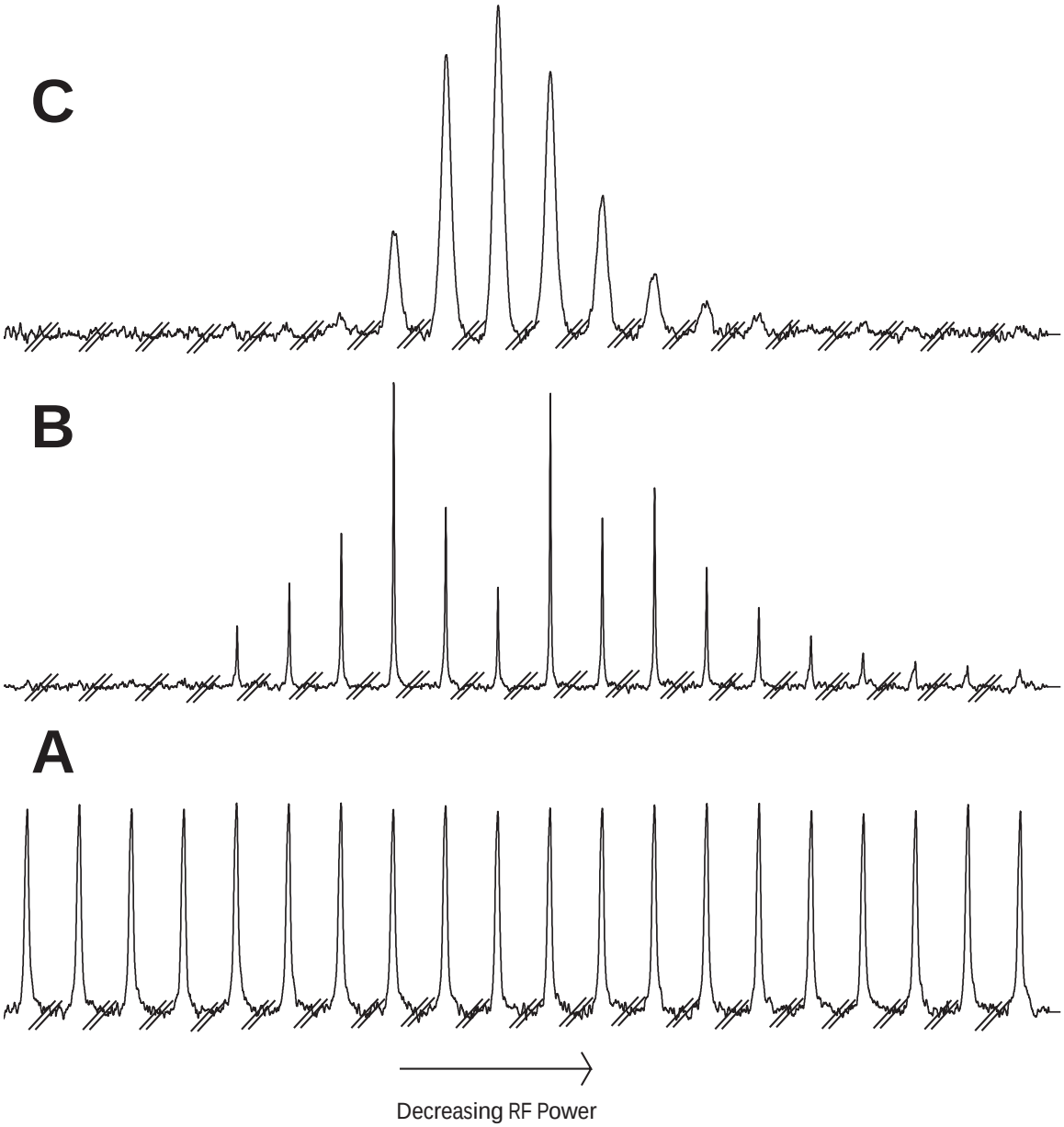


Figure 14: The $^{13}C$ CP/MAS signal response of a single peak in the spectrum repeatedly plotted as the $^{13}C$ amplifier gain is decreased in twenty steps of 0.25 dB each from left to right. A decibel is a relative measure of power and is given by $10*\log_{10}(P/P_0)$. The top trace (C) shows the upfield methine resonance of a static sample of adamantane while the middle spectrum (B) shows the same upfield methine resonance of adamantane for a sample spinning at 3 kHz. The bottom spectrum (A) shows the methylene resonance of α-glycine spininng at 5 kHz similarly acquired.

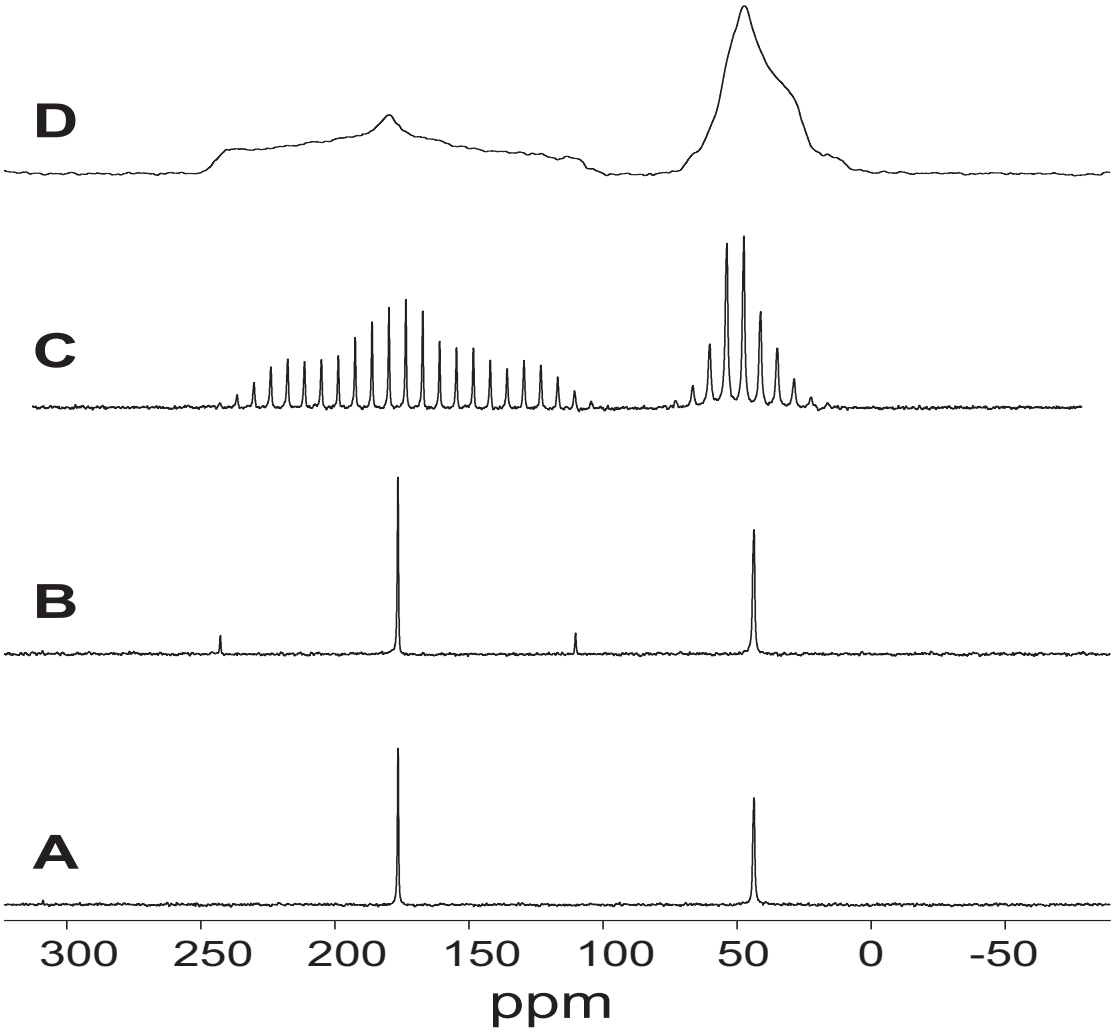


Figure 15: $^{13}C$ cross-polarization spectra of α-glycine as a function of rotation speed: a) 10,000 Hz, b) 5,000 Hz, c) 500 Hz, and d) static sample. The data were acquired with a $^{1}H$ 90 degree pulse width of 3.75 μs, a Hartmann-Hahn contact time of 3 ms, and a recycle delay of 3 s. The dwell time was 16 μs with an acquisition time of 65 ms.

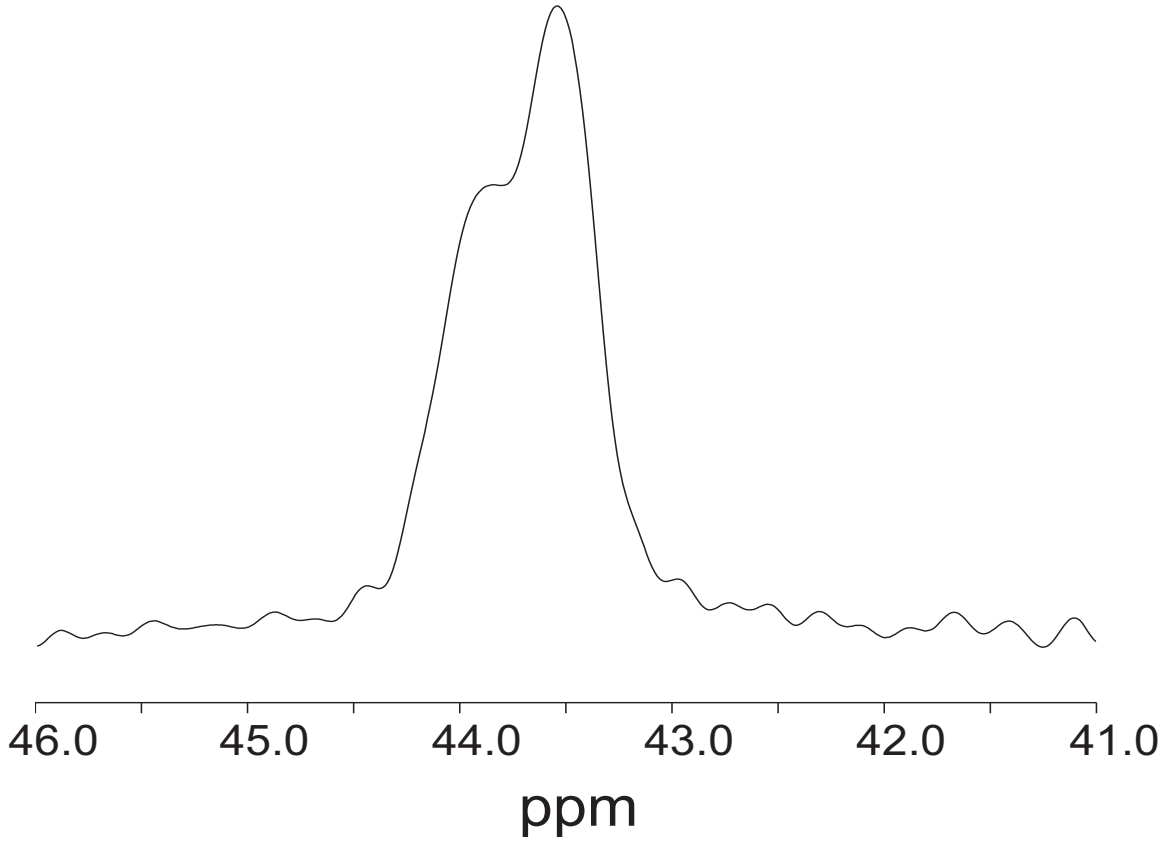


Figure 16: $^{13}C$ CP/MAS spectrum of the alpha carbon of α-glycine acquired in a magnetic field of 7.0 Tesla ($^{1}H$ at 300 MHz). The single asymmetric resonance is due to the dipolar coupling of the quadrupolar $^{14}N$ to the $^{13}C$. The $^{1}H$ 90 degree pulse was 3.75 μs with a Hartmann-Hahn contact time of 3 ms. A dwell time of 16 μs was used. The sample rotation speed was 5 kHz.

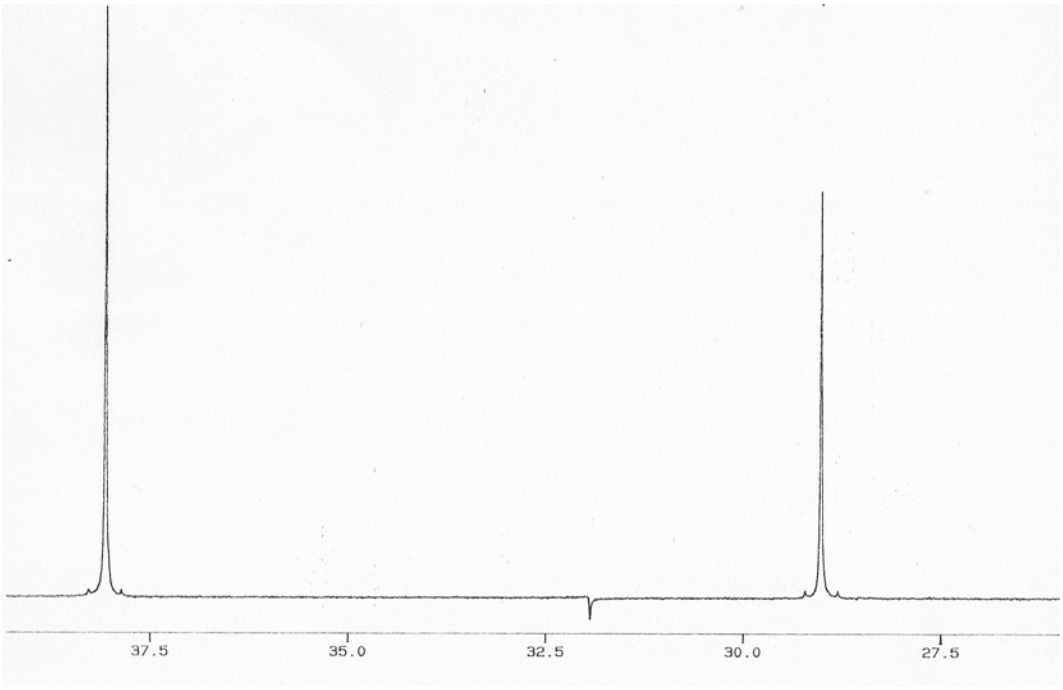


Figure 17: $^{13}C$ CP/MAS spectrum of adamantane with a full width at half height of 1.8 Hz. The $^{13}C$-$^{13}C$ satellites with a scalar coupling of 31.6 Hz are visible at the base of each peak. The spectrum was acquired with a 6 μs $^{1}H$ 90 degree pulse with a Hartmann-Hahn contact time of 5 ms. A dwell time of 66 μs was used with at total acquisition time of 950 ms. The small peak at 32 ppm is a quadrature image caused by small imbalances in the amplitudes and/or small deviations from the ninety degree phase separation of the two receiver channels.

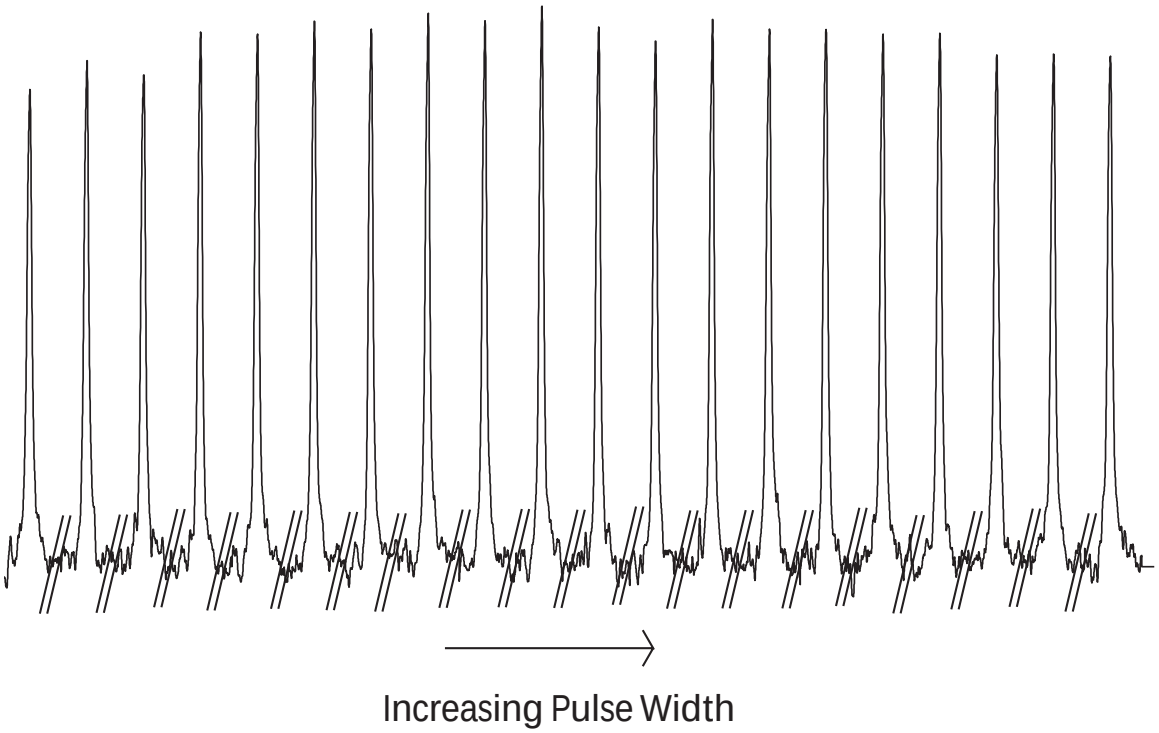


Figure 18: The $^{13}C$ CP/MAS spectrum of the methylene carbon of $\alpha$-glycine plotted twenty times as the pulse width for the TPPM decoupling sequence is incremented by 0.1 $\mu$sec from the pulse width of 5.7 $\mu$sec for the peak on the left. The acquisition conditions are the same as Figure 15.

Robert E. (Bob) Taylor earned his Ph.D. in 1980 working on the development of the Combined Rotation and Multiple Pulse Spectroscopy (CRAMPS) technique in the laboratory of Professor Bernie Gerstein in the Department of Chemistry at Iowa State University in Ames. For a number of years he worked as an analytical NMR spectrosocpist applying solution-state, solid-state, and microimaging techniques to problems in the petrochemical and agricultural chemical industries. Seeking to escape the vagaries of corporate America, he joined what was then Bruker Instruments Incorporated as an applications scientist to see the world....and did. Growing weary and giving up his frequent flier miles, he left Bruker to work in the NMR Facility of the Chemistry Department at Texas A&M University. Upon realization that one must actually graduate from A&M to be a true Aggie, he left in 2001 for his current position in the NMR Facility in the Department of Chemistry and Biochemistry at the University of California, Los Angeles. His areas of responsibility include solid-state NMR and EPR.